# Travelling Modes in Wave-Heated Plasma Sources

John Phillip Rayner and Andrew Desmond Cheetham, *Member, IEEE*

*Abstract*—This paper describes a theoretical and experimental study of surface- and helicon-wave-heated plasma sources in which standing waves are set up in the cavity between the closed end plate to a plasma vessel and a wave launcher while travelling waves propagate from the opposite side of the launcher into a region which is long compared with the attenuation distance of the waves. We model the situation as a lossy transmission line of finite length coupled at the launcher to a lossy transmission line of infinite extent. RF power applied to the launcher divides in the ratio of the input impedances of the two transmission lines. For a conducting end plate, the power delivered to the travelling waves is a maximum when the cavity length is an odd number of 1/4 wavelengths long for which its input impedance is a maximum. Similarly, for an insulated end plate, the power delivered to the travelling waves is a maximum for a cavity with a length equal to an integer number of half wavelengths for which its input impedance is again a maximum.

*Index Terms*—Helicon waves, plasma heating, plasma waves, standing-wave measurements, surface waves, travelling-wave devices.

## I. Introduction

SEVERAL STUDIES have investigated standing-wave modes in cylindrical plasma sources closed at both ends [1]–[4]. In this paper, we report on two studies of cylindrical plasma sources with a geometry involving one closed end, an antenna to launch the waves, and an essentially free end well removed from the antenna. The first study relates to a plasma excited by a surface-wave discharge in a vessel with an insulating closed end. This geometry is relevant to surface-wave sources used for processing purposes [5] or plasma antennas [6], [7]. The second study involves a helicon source with a conducting closed end. This geometry is relevant to plasma applications where a wave-heated source is attached to a separate processing chamber [8], [9, p. 417]. In each of these applications, standing waves are established in the "cavity" between the antenna and the closed end, while travelling waves propagate toward the free end. Thus, in plasma processing applications, the source is often coupled to a processing chamber, with the object to be processed located in the travelling-wave field which propagates into the processing chamber. Similarly, for a plasma antenna

excited from near to one end, the plasma column that forms the antenna is generated by the travelling wave. In each case, the intention is to maximize the power delivered to the travelling waves.

The aim of this paper is to demonstrate that the power delivered to the free end is a maximum when constructive interference occurs between the wave transmitted directly to the plasma and the wave reflected from the end of the cavity. Thus, if the end of the cavity is an insulating open circuit, it is expected that maximum power should be delivered to the plasma column when the length of the cavity is an integer multiple of half a wavelength. Similarly, if the end of the cavity is a conducting short circuit, then the power delivered should be a maximum when the length of the cavity is an odd number of quarter wavelengths. The waves heat the plasma as they propagate and so attenuate, which means that the interference effect should become weaker as the length of the cavity increases, since the waves in the cavity traverse a greater distance before they reflect back to the launcher.

The situation described here has many similarities with a lossy transmission line where power is fed into the line at a finite distance from one end of the line. The fraction of the applied power that propagates along the line depends on the distance of the feed point from the end of the line and the nature of the termination, i.e., an open or short circuit. Section II of this paper develops a general theory based on this idea.

Two experimental investigations have been undertaken to test this hypothesis. Section III describes a surface-wave discharge produced in a cylindrical geometry with an insulating end cap in which the wave launcher was moved with respect to the end cap while recording the length of the cavity and the length of the free plasma column. Section IV describes a helicon source in which a metal baffle was moved with respect to the antenna launching the helicon waves while monitoring the amplitude of the travelling waves using a set of B-dot coils. Section V draws some general conclusions relevant to both types of discharges.

## II. Theory

### A. General Considerations

Fig. 1 shows a wave-heated plasma discharge where the wave launcher (antenna) is located toward one end of the plasma column.

The region between the launcher and the closed end acts as a cavity of length $l$ that we model as a lossy transmission line terminated in either an open or short circuit, depending on whether the end is an insulator or a conductor.

The free end of the plasma column is shorter than the overall length of the plasma vessel due to absorption of the wave energy
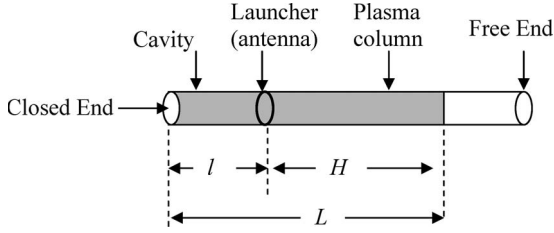
Fig. 1.   Geometry of the plasma vessel.

by the plasma. There are, therefore, no reflections from the free end of the vessel, and so, we can model the column in the free region as a very long lossy transmission line. For the surface-wave discharge, the end of the plasma column is fairly well defined, giving it an effective length $H$.

We assume that the RF power applied to the launcher splits into a component that heats the plasma in the cavity and a second component that heats the free plasma column. The ratio in which the power splits depends on the ratios of the impedance presented to the launcher by the cavity and the column. As the length of the cavity increases, its impedance varies as a function of $l$ in a similar way to the input impedance of a lossy transmission line of finite length terminated in a short (or open) circuit, while the impedance of the free plasma column remains constant. The power applied to the column therefore varies in a periodic fashion as the length of the cavity increases. Earlier work with surface-wave discharges [7] showed that the length of a plasma column varied as the square root of the applied power. Hence, it may be expected that the length of the column should vary periodically as the length of the cavity increases. In particular, if the cavity impedance is high, then most of the power will be directed to the column which will therefore be long. If the cavity impedance is low, then most of the power will be directed to the cavity with a consequently short column.

In addition to the variation in the ratio of the power split, the total impedance of the parallel combination of the cavity and column and the intrinsic impedance of the launcher will vary as a function of cavity length. Thus, even if the RF source is matched to the total impedance at a particular cavity length and if there is no retuning of the matching network, the power delivered to the antenna will vary in a periodic fashion as the cavity length increases.

As the cavity length increases, the effect of its finite length will become less noticeable due to the absorption of the wave. Eventually, as the cavity length becomes comparable to the absorption length of the waves, then the cavity will appear as a pure constant impedance, the variation in the power ratio will disappear, and the plasma column will remain of constant length. This situation can arise even though the length of the cavity is less than the length of the free column since absorption in the cavity occurs for both the incident and reflected waves. Eventually, as the cavity becomes very long, the plasma fails to reach the end of the vessel so that free columns form on both sides of the launcher.

For both surface and helicon waves, the observed attenuation coefficients $\alpha$ is small compared with the phase constant $\beta$. For the surface waves, $\alpha/\beta \sim 0.05$, while for the helicon
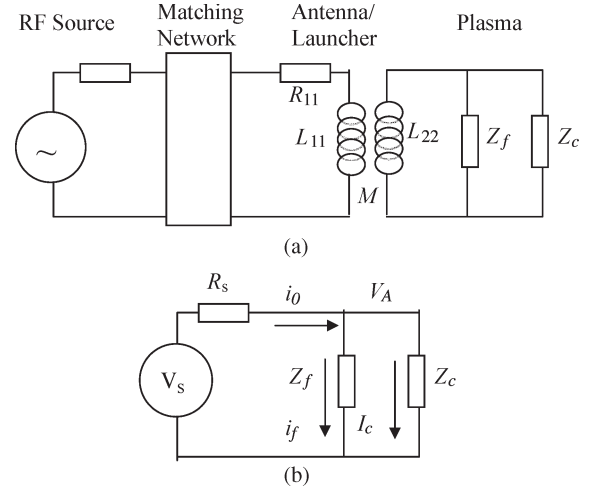




Fig. 2.   (a) Electrical model of the RF source, cavity, and free column. (b) Thevinin equivalent circuit for the plasma.

waves, $\alpha/\beta \sim 0.1$. Therefore, for both types of waves, we model the cavity and the free column as low-loss transmission lines of characteristic wave impedance $\eta = \eta_R + j\eta_I$, where $\eta_R$ is the characteristic resistance and $\eta_I$ is the characteristic reactance. For a low-loss line, $\eta_I/\eta_R \leq \alpha/\beta$, and we assume that the reactance may have a finite effect particularly for the helicon discharge where values of $\alpha/\beta$ up to $\sim$0.3 have been reported [10]. For the surface wave, however, since $\alpha/\beta \ll 1$, we assume $\eta_I = 0$ as was also assumed by Moison and Zakrzewski [5].

It should be noted that $\eta$ is not the same as the antenna impedance $Z_A$ "seen" by the matching network as $Z_A$ also includes the resistance and reactance of the antenna itself, plus the plasma impedance reflected back into the antenna by, for example, transformer action in the case of the helicon discharge [11]. This impedance may include not only the wave impedance but also the inductive reactance of the secondary of the transformer [11].

Fig. 2(a) shows a model of the electrical system consisting of the RF source, matching network, launcher (antenna), and plasma drawn for the helicon discharge. Since we are only interested in the division of power between the cavity and the free column within the plasma, we can replace most of the network by a Thevenin equivalent voltage source within the plasma as shown in Fig. 2(b). The impedance $Z_f = R_f + jX_f$ represents the impedance of the free column, while $Z_c = R_c + jX_c$ represents the impedance of the cavity.

$V_s$ is the open-circuit output voltage of the RF generator of output resistance $R_s$, while $V_A$ is the voltage applied to the inputs to the cavity and the free column.

The magnitude of the cavity current is given by

$$i_c = \frac{V_A}{|Z_c|} \tag{1}$$

with power dissipation

$$P_c = |i_c|^2 R_c = \frac{V_A^2 R_c}{|Z_c|^2} \tag{2}$$

while for the column

$$P_f = \frac{V_A^2 R_f}{|Z_f|^2} \qquad (3)$$

where the total net power at the antenna $P_{TA}$ is simply expressed as

$$P_{TA} = P_f + P_c. \qquad (4)$$

Combining (1)–(4) leads to the following expression for the power delivered to the free column:

$$\frac{P_f}{P_{TA}} = \frac{1}{1 + \left(\frac{R_c}{R_f}\frac{|Z_f|^2}{|Z_c|^2}\right)}. \qquad (5)$$

For a lossy transmission line of length $l$, the input impedance is given by [12, p. 451]

$$Z_i = \eta\left(\frac{Z_L + \eta\tanh\gamma l}{\eta + Z_L\tanh\gamma l}\right) \qquad (6)$$

where $\eta$ is the (complex) characteristic impedance of the line, $Z_L$ is the load impedance, and $\gamma$ is the propagation constant given by

$$\gamma = \alpha + j\beta \qquad (7)$$

with $\alpha$ being the attenuation constant and $\beta$ being the phase constant. The use of a complex characteristic impedance allows for the existence of resistive and reactive components for both the surface and helicon waves.

### B. Cavity With Short-Circuit Termination

For the helicon-wave experiments, the end of the cavity is a conductor for which we can assume that it is terminated by a short-circuit load impedance $Z_L \to 0$.

Hence, from (6), the metal end leads to a short-circuited transmission line for the cavity of input impedance

$$Z_c = \eta\tanh\gamma l. \qquad (8)$$

If we define

$$T(\gamma l) = \tanh(\gamma l) = T_R + jT_I \qquad (9)$$

where

$$T_R = \frac{\tanh\alpha l\,\sec^2\beta l}{1 + \tanh^2\alpha l\,\tan^2\beta l} \qquad (10)$$

$$T_I = \frac{\tan\beta l\,\operatorname{sech}^2\alpha l}{1 + \tanh^2\alpha l\,\tan^2\beta l} \qquad (11)$$

then

$$Z_c = \eta T(\gamma l) = (\eta_R + j\eta_I)(T_R + jT_I). \qquad (12)$$

Thus, the cavity resistance becomes

$$R_c = \eta_R T_R\left(1 - \frac{\eta_I}{\eta_R}\frac{T_I}{T_R}\right). \qquad (13)$$

Similarly

$$X_c = \eta_R T_I\left(1 + \frac{\eta_I}{\eta_R}\frac{T_R}{T_I}\right). \qquad (14)$$

For the free column, since there are no reflections

$$Z_f = R_f + jX_f = \eta = \eta_R + j\eta_I. \qquad (15)$$

If (12), (13), and (15) are substituted into (5), then the fraction of the total power applied to the travelling waves in the free column under short-circuit conditions is given by

$$\frac{P_{fs}}{P_{TA}} = \frac{1}{1 + \left(\frac{T_R}{T_R^2 + T_I^2}\right)\left(1 - \frac{\eta_I}{\eta_R}\frac{T_I}{T_R}\right)} \qquad (16)$$

where the subscript "$fs$" refers to the power delivered to the free column when the end of the cavity is a short circuit.

If we examine (16) in the limit of very short cavities, then, as $l \to 0$, $T_R \to \alpha l$, $T_I \to \beta l$, and

$$\frac{P_{fs}}{P_{TA}} \to \frac{1}{1 + \frac{\alpha}{\beta}\frac{1}{\beta l}\left(1 + \frac{\alpha^2}{\beta^2}\right)^{-1}\left(1 - \frac{\beta}{\alpha}\frac{\eta_I}{\eta_R}\right)} \qquad (17)$$

(17) shows that, in order to keep the power delivered to the column less than the total power, it is necessary that

$$\frac{\eta_I}{\eta_R} < \frac{\alpha}{\beta}. \qquad (18)$$

This result is consistent with classical low-loss transmission lines [12, pp. 442] where, in terms of the inductance $L$, capacitance $C$, conductance $G$, and resistance $R$, per unit length, the ratio of the characteristic reactance to its resistance is given by $X_0/R_0 = (\alpha/\beta)((1 - \delta)/(1 + \delta))$, with $\delta = (RC/GL) = (R/R_0)(1/R_0 G)$.

If (18) is satisfied, then, as $l \to 0$, $P_{fs}/P_{TA} \to 0$, which means that all of the power is dissipated in the short-circuit cavity.

In the limit where the cavity becomes very long, $T_R \to 1$, $T_I \to 0$, and $P_{fs}/P_{TA} \to 1/2$ so that the power divides equally between the cavity and the free column.

The amplitude of the travelling helicon waves is proportional to the square root of the applied power. Since the power applied to the travelling waves is a function of the length of the cavity through $T_R$ and $T_I$, we might therefore expect that the amplitude of the travelling waves should vary as the length of the cavity increases.

### C. Cavity With Open-Circuit Termination

For the surface-wave experiments, the end of the cavity is an insulator for which we can assume that it is terminated with an

open-circuit load impedance $Z_L \rightarrow \infty$. Thus, (6) becomes

$$Z_c = \frac{\eta}{\tanh \gamma l} = \frac{\eta}{T_R + jT_I}. \qquad (19)$$

Proceeding in the same way as above, we find that the power delivered to the free column for an open-circuit (insulating end) cavity is given by

$$\frac{P_{f0}}{P_{TA}} = \frac{1}{1 + T_R \left(1 + \frac{\eta_I}{\eta_R} \frac{T_I}{T_R}\right)} \qquad (20)$$

where the subscript "$f0$" refers to the power delivered to the free column when the end of the cavity is an open circuit.

In this case, as $l \rightarrow 0$, $P_{f0}/P_{TA} \rightarrow 1$, so that all of the power is dissipated in the free column.

For a plasma heated by a surface wave, the length $H$ of the plasma column measured from the launcher increases as the square root of the applied power [7], i.e.,

$$H = C\sqrt{P_c} \qquad (21)$$

where $C$ is a constant with a value $\sim 10$ cm/W$^{1/2}$ for the fluorescent tube used as an antenna in [7]. The length of the free column is therefore a useful measure of the power supplied to the travelling waves, and therefore, from (20), we might expect that the length of the column should vary in a regular way as the length of the cavity increases via the functions $T_R$ and $T_I$.

## III. SURFACE-WAVE DISCHARGE

### A. Experimental Setup

The surface-wave experiments were conducted using a domestic fluorescent tube, 25 mm in outer diameter and 1.2 m long, filled with argon at a nominal pressure of 0.4 mbar and a small amount of mercury vapor. The metal end cap was removed so that the closed end of the tube was essentially a glass insulator apart from the very fine metal filament wire. The simple launcher for the surface waves consisted of a square ground plane of side 50 mm, perpendicular to the column, and a collar of length 25 mm, located on the cavity side of the ground plane, with a gap of 1.0 mm between the ground plane and the collar. The launcher could be slid readily along the tube, thus changing the length of the cavity between the end cap and the launcher. The RF power applied to the collar was sufficient to maintain a plasma in the cavity, but not enough to completely fill the other end of the tube, thus producing an essentially free end. RF power up to 100 W at frequencies between 0.5 and 1.0 GHz was employed to excite the plasma via a double-stub matching unit. A directional power meter monitored the forward- and reverse-power. For each position of the launcher, the matching unit was adjusted to minimize the reflected power, thus keeping the net power applied to the launcher essentially constant. For an input power of 100 W, the reflected power following adjustment of the matching unit was typically <1–2 W. The length of the plasma column from the launcher was measured for each position of the launcher at constant net input power.
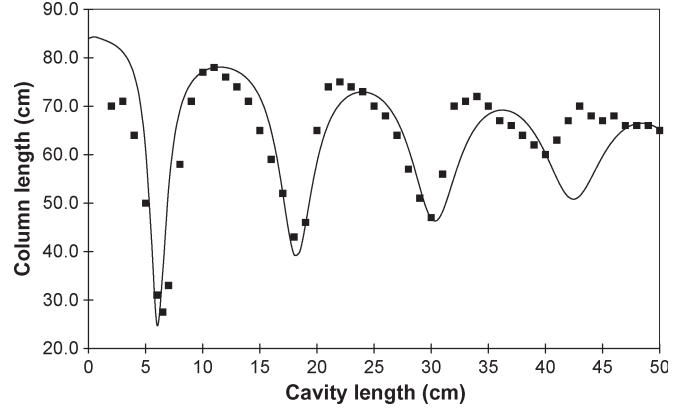


Fig. 3. Length of the plasma column from the launcher as a function of column length for a fluorescent tube (filled with argon/mercury vapor at a pressure of $\sim$0.4 mbar, with an RF power of 65 W and a frequency of 1.0 GHz). The fitted theoretical length is shown for comparison

### B. Results and Discussion: Surface-Wave Source With an Insulating End Cap (Open-Circuit Termination)

*1) Column Length:* Fig. 3 shows the experimental data for the length $H$ of the plasma column in the fluorescent tube, measured from the launcher as a function of cavity length for a fixed input power of 65 W at a frequency of 1.0 GHz. The anticipated periodic variation in the length of the column is clearly evident. The amplitude of the oscillations decreases as the length of the cavity increases due to the increasing attenuation of the waves in the cavity, and consequently, when they return to the launcher, their reduced influence, on the travelling waves. The oscillations disappear at a cavity length of $\sim$45 cm as the plasma no longer reaches the end of the cavity. For further increases in cavity length the free column length remains constant at $\sim$65 cm. The difference in the lengths is due to the asymmetry in the geometry of the launcher.

The figure also shows the theoretical variation in column length based on (20) and (21). In general, the theoretical curve reproduces the main features of the experiment with large oscillations and sharp minima when the cavity is short and there is a strong interaction between the reflected waves and the travelling waves. As the length of the cavity increases, the increased attenuation of the reflected waves results in smaller oscillation and broader minima.

In making this comparison, the wavelength, and hence $\beta$, is based on a wavelength of 24.5 cm that is equal to twice the average spacing between the dips in the experimental plot. In addition, the value of the attenuation coefficient $\alpha$ was adjusted to give an optimum fit between theory and experiment. The final value chosen of $\alpha = 0.015$ cm$^{-1}$ corresponds to an attenuation distance of 67 cm. Similar observations were made for RF frequencies of 0.5, 0.625, 0.75, and 0.875 GHz. For each data set, a theoretical curve was fitted to the results, leading to an experimental wavelength and attenuation coefficient for each frequency.

To test the proposition that the length of the column is a maximum if the length of the cavity is an integer number of half wavelengths long, the cavity length for each maximum, measured between the geometrical end of the tube and the ground plane of the launcher, was recorded and divided by
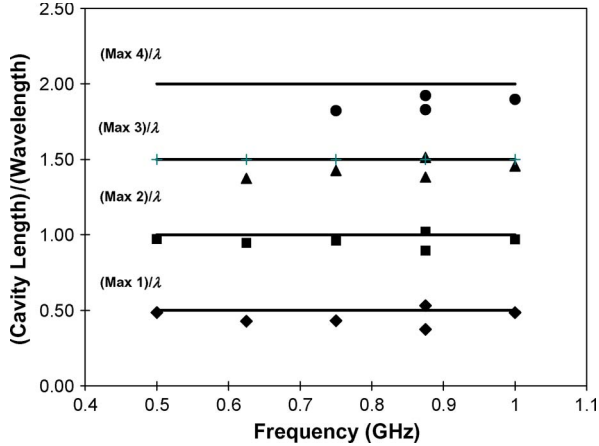
Fig. 4.   (Cavity length for which the column length is a maximum)/(wavelength) as a function of frequency for the first four maxima.

the average wavelength, determined by the average distance between minima, for each frequency. Similarly, the length for each minimum was treated in the same way. Fig. 4 shows some typical results that clearly show that the length of the column is a maximum for

$$l = n \left( \frac{\lambda}{2} \right), \qquad \text{where } n = 1, 2, 3, \ldots \qquad (22)$$

Results with a comparable amount of scatter confirmed that, for a minimum

$$l = (2n - 1)\frac{\lambda}{4}, \qquad \text{where } n = 1, 2, 3, \ldots . \qquad (23)$$

*2) Wavelength Comparisons:* The dispersion relation for a surface wave in a cylindrical geometry is given by [9, p. 446]

$$\frac{\kappa_p I_0'(\alpha_p a)}{\alpha_p a I_0(\alpha_p a)} = \frac{\kappa_d K_0'(\alpha_d a)}{\alpha_d a K_0(\alpha_d a)} \qquad (24)$$

where $K_0$ and $I_0$ are modified Bessel functions of the first and second kind, the primes denote their derivatives, and

$$\alpha_d^2 = k_z^2 - \kappa_d k_0^2 \qquad (25)$$

$$\alpha_p^2 = k_z^2 - \kappa_p k_0^2 \qquad (26)$$

$$\kappa_p = 1 - \frac{\omega_{pe}^2}{\omega(\omega - j\nu_m)} \qquad (27)$$

with $\kappa_p$ being the dielectric constant of the plasma and $\kappa_d$ being the dielectric constant of the surrounding medium.

For the conditions encountered in these experiments, $(\nu_m/\omega)^2 \ll 1$, and so, (24) was solved numerically in this limit for the wavenumber $k_z$ as a function of the electron number density $n_e$ for frequencies between 0.5 and 1.0 GHz for a column with a diameter of 2.4 cm. It was also assumed that $\kappa_d = 1$ because of the small effect of the very thin glass walls of the fluorescent tube. Under these conditions and for the range of
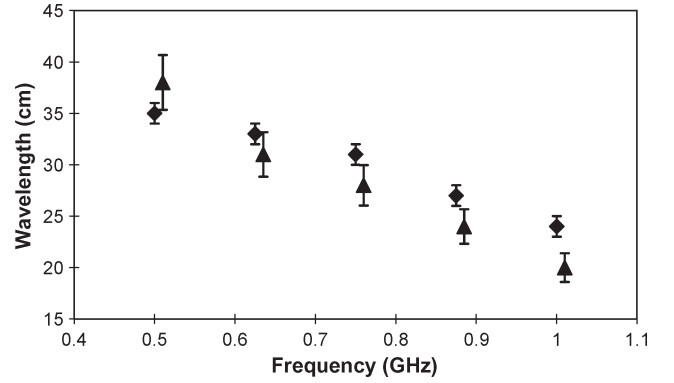


Fig. 5.   (Diamonds) Measured wavelength for different RF frequencies compared with (triangles) the wavelength found from interferometer measurements of the number density and the surface-wave dispersion relation. Note that, for clarity, the results based on the dispersion relation have been offset by 0.1 GHz.

number densities of interest, we find that the dispersion relation can be approximated by an expression of the form

$$k_z = k_0 \left( 1 + a \left( \frac{n_0}{n_e} \right)^b \right) \qquad (28)$$

where $a \approx 0.1$ and $b \approx 1.0$ are constants that are weak functions of $\omega$ and $n_0 = 10^{18}$ m$^{-3}$ is a reference density. Between 0.5 and 1.0 GHz, $a$ increased from 0.092 to 0.12 while $b$ increased from 0.95 to 1.05.

A microwave interferometer operating at 9.5 GHz measured the electron number density at a point half way along the cavity for a cavity length corresponding to the first maximum in column length after the initial minimum. For example, in Fig. 3, the measurement was made at a point 6 cm from the end cap. This point was selected as being indicative of typical conditions within the cavity. The densities were measured in the cavity, rather than in the free column, since it is the wavelengths within the cavity which are important in this study and which depend on the cavity density. The number densities were line-averaged values obtained from the interferometer measurements, assuming a parabolic density profile across the plasma column. The densities increased in an approximately linear way from $1.6 \times 10^{17}$ m$^{-3}$ at 0.5 GHz to $4.2 \times 10^{17}$ m$^{-3}$ at 1.0 GHz. From (28), $k_z/k_0$ therefore ranged from about 1.63 at 0.5 GHz down to 1.23 at 1.0 GHz. These figures show that increasing the density by a factor of 2.6 decreases $k_z/k_0$ by $\sim 30\%$, which indicates that, for the range of densities encountered in these experiments, the wavelength was a fairly weak function of density.

Fig. 5 compares the observed wavelengths with wavelengths inferred from the interferometer measurements of the number density and the dispersion relation. The error bars on the measured wavelengths reflect the variation in the position of successive minima in the pattern. The error bars on the wavelengths based on the dispersion relation are due to uncertainties in the measurements of the interferometer's phase shifts. The two sets of wavelengths generally lie within the error bars of the observations, although there may be a systematic difference at higher frequencies, possibly due to the assumptions made in the analysis of the interferometer's data.

*3) Attenuation Comparisons:* The attenuation coefficient as a function of plasma electron density can be approximated by an expression of the form [5]

$$\alpha(n) = \frac{B(\omega, a)\nu_m}{n - n_{\text{res}}} \quad (29)$$

and the number density variation along the plasma column as [7]

$$n = n_{\text{res}} + B(\omega, a)\nu_m(H - z) \quad (30)$$

where $H$ is the height of the column, $z$ is the distance along the column measured from the launcher, $\nu_m$ is the electron–neutral collision frequency for momentum transfer, $n$ is the average number density of electrons, and $n_{\text{res}}$ is the number density for a plasma frequency $\omega_{pe}$, corresponding to the frequency of the RF source, modified by the dielectric constant $\kappa_d$ of the surrounding insulating medium (e.g., glass or air), and given by

$$n_{\text{res}} = (1 + \kappa_d)\frac{\varepsilon_0 m_e \omega^2}{e^2}. \quad (31)$$

Thus, from these equations

$$\alpha(z) = \frac{1}{(H - z)} \quad (32)$$

or, at the launcher

$$\alpha(0) = \frac{1}{H}. \quad (33)$$

The free length of the plasma column should therefore give a measure of the attenuation coefficient for the cavity.

Fig. 6 shows the attenuation coefficients used to fit the theoretical curve to the experimental results for each frequency. For comparison, it also shows the attenuation coefficient estimated from the maximum free length of the plasma column using (33). The error bars on the fitted attenuation coefficients represent the sensitivity of their values to the quality of the fit. The error bars on the estimated values relate to uncertainties in determining the effective end of the plasma column. The generally good agreement between the two sets of data confirms that the free length of the plasma column can be used to obtain a useful estimate of the attenuation coefficient.

*4) Wavelength Variation With Cavity Length:* The experiments and theory presented so far have accounted for the main features of the interaction between the cavity and the free column. There is some evidence, however, for example, in Fig. 3, that as the length of the cavity increases, the distance between the minima decreases from ∼12 to ∼10 cm, implying some decrease in wavelength from ∼24 to ∼20 cm. Similarly, in Fig. 4, the ratio of cavity length to wavelength is consistently less than the expected ratio for long cavities where, for a given frequency, a constant wavelength has been used to calculate the ratio. If, however, the wavelength decreases as the cavity length
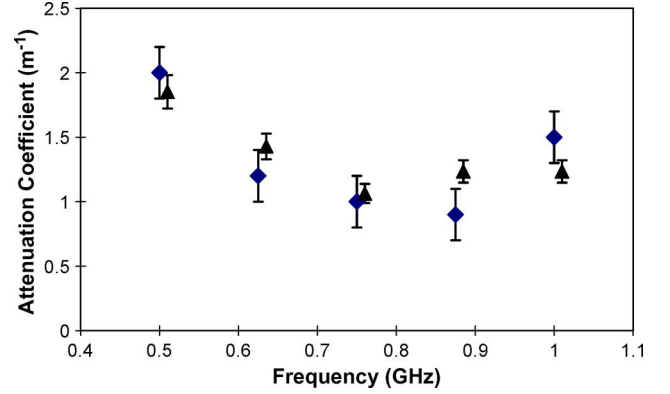


Fig. 6. (Diamonds) Fitted attenuation coefficient compared with the attenuation coefficient estimated from the free length of the plasma column as a function of frequency. Note that, for clarity, the estimated values have been offset by 0.01 GHz.

increases, then the ratio using the decreasing wavelength should increase to some extent.

The decease in wavelength with increasing cavity length may be explained by noting that, for short cavities, both the incident and reflected waves heat the plasma, producing high electron densities. For long cavities, however, most of the heating is only by the incident wave and takes place over a longer distance. The average power density in the cavity therefore decreases with a consequent decrease in the electron number density. From the dispersion relation (28), the wavelength should therefore decrease, and the attenuation coefficient (29) should increase.

An estimate of the magnitude of this effect on wavelength can be made by assuming that the power delivered to the cavity is the difference between the total power $P_{TA}$ and the power delivered to the column which can be estimated from (21). If the volume of a cavity of length $l$ is $Al$, where $A$ is its cross-sectional area, then the average power density $P_D$ is given by

$$P_D = \frac{P_{TA} - (H/C)^2}{Al}. \quad (34)$$

If we also assume that the electron number density is proportional to the power density and that the electron densities are measured with respect to a reference density $n_0$ measured by the interferometer at a reference cavity length $l_0$, then we can estimate the variation in electron density with cavity length. If we substitute these densities in the approximate dispersion relation (28), we can find the wavelength as a function of cavity length.

Fig. 7 shows the results of this calculation which indicate that the wavelengths decrease from ∼24 to ∼20 cm with increasing cavity length, which is consistent with the experimental results in Fig. 3.

Fig. 7 also shows the attenuation coefficient based on (29) as a function of cavity length using the same number densities. It shows that the attenuation should increase with a consequent increase in the damping of the oscillations in Fig. 3 for long cavities compared with the theoretical damping with a constant attenuation coefficient.
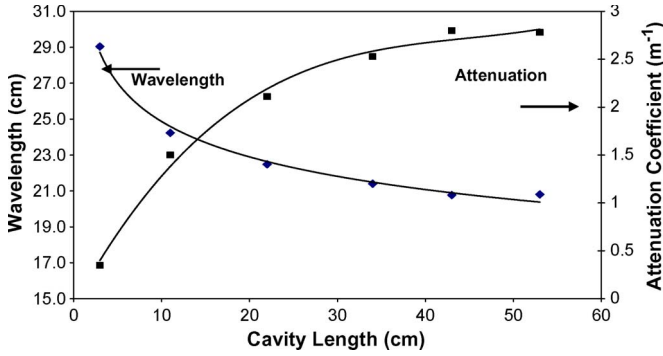
Fig. 7. Theoretical variation in wavelength and attenuation coefficient as functions of the cavity length at 1.0 GHz, assuming that the electron density in the cavity is proportional to the average power density.

## IV. HELICON WAVES

### A. Experimental Setup

The helicon-wave experiments were conducted in the PR3 plasma source shown in Fig. 8. The source consisted of a Pyrex vacuum vessel, 10 cm in diameter and 160 cm in length, with a central region that is 105 cm long for which an adjustable axial magnetic field of 0–600 G was uniform to within ±4%. For this investigation, all measurements were taken at a field of 400 G. One end of the vessel had a metal end plate located 10 cm beyond the end of the uniform field region and 54 cm from the centrally located antenna. The other end of the vessel had a glass end cap located 45 cm beyond the uniform field region and 96 cm from the antenna. A stainless steel shaft carried a moveable stainless steel mesh baffle that could be moved axially under vacuum, thus providing cavity lengths, within the uniform field region, in a range from 15 cm to 45 cm between the baffle and the center line of the antenna. The shaft also carried a Langmuir probe whose tip was located on the axis of the vessel and 10.0 cm in front of the baffle. The probe therefore sampled the plasma at a point representative of conditions in the cavity region. This point was chosen because it was the conditions in the cavity region, which determined the wavelengths of the waves in the cavity. The interaction of these reflected waves with the directly transmitted waves then determined what happened in the free column. The glass end cap on the other end of the vessel was far enough from the antenna, and outside the region of uniform magnetic field, for wave reflections not to occur. The plasma was excited by an $m = 1$ Boswell helicon antenna [1] with a length of 11 cm fed via a balanced transformer and matching network at 13.56 MHz and RF power levels up to 2.8 kW [13]. The working gas was argon with pressures between 2 and 4 $\mu$bar.

A moveable array of four pick-up coils connected to a digital oscilloscope measured the amplitude of the azimuthal magnetic field component of the helicon waves as a function of axial distance along the plasma vessel. Each coil consisted of two windings, of four turns each, wound in opposite directions on a 4-mm-diameter former. A balanced transformer subtracted the outputs from the windings, thus cancelling the common mode pick-up from the electric fields while summing the magnetic fields. The array, with a typical coil spacing of 8 cm, could be placed to monitor either the cavity region or the free region.

All measurements were made within the uniform magnetic field region. Observation of the phase of the signals from the axial array clearly demonstrated the presence of standing waves in the cavity region and travelling waves in the free region. Excitation of one coil by an external signal generator at 13.56 MHz while monitoring the other coils confirmed that the coupling between the coils was negligible for the coil-spacings employed.

### B. Results and Discussion: Helicon-Wave Source With a Conducting End Plate (Short-Circuit Termination)

1) Wavelength Data: Fig. 9(a) shows some typical results for the travelling waves in the free region recorded between 20 and 44 cm from the center line of the antenna but within the region of uniform axial magnetic field. In many cases, the signals exhibited a significant third harmonic component in addition to the fundamental shown in Fig. 9(b). Wavelengths were obtained from these signals and also from the standing waves in the cavity region for a range of pressures and RF power levels. In general, the wavelengths found from the standing waves were found to be consistent with those obtained from the travelling waves under similar conditions of RF power level, field, and pressure.

The amplitudes of the signals for a given set of conditions were of similar magnitude, indicating that little attenuation occurred over the distance of 24 cm spanned by the coils, which is of the same order as the half wavelength of the helicons. These observations helped to confirm our initial assumption that both the surface wave and helicon discharges could be modeled as low-loss lines.

2) Wavelength Measurements: Since conditions were often unstable, close to sudden transitions from one standing-wave mode to another, an indirect means of determining the wavelength was also employed using the helicon dispersion relation [9, p. 437] and the expression for the saturation ion current for the Langmuir probe [9, p. 174]. If these two expressions are combined, and $k_\perp \gg k_z$, then, for our probe, the wavelength $\lambda$ (in centimeters) is related to the ion current $I_i$ (in milliamperes) by

$$\lambda I_i = 5.87 \times 10^{-2} B_0 \chi \sqrt{T_e} \qquad (35)$$

where the electron temperature $T_e$ is in electronvolts, the axial magnetic field $B_0$ is in Gauss, and, for the lowest order radial mode, $\chi = 3.1$.

Numerous simultaneous measurements of wavelength and ion current showed that

$$\lambda I_i = K \qquad (36)$$

where $K = 150 \pm 12$ cm · mA is a constant compared with a theoretical value of 140 cm · mA based on (35) for our conditions ($B_0 = 400$ G, $T_e = 3.5$ eV). In making this comparison, the electron temperature is a theoretical value based on a previously tested global model of the plasma source [14]. Wavelengths close to a transition could therefore be inferred based on the value of the ion current close to the transition.
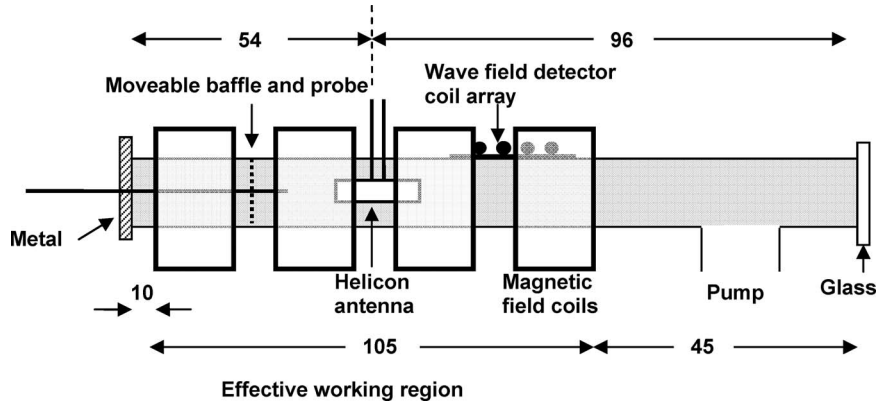
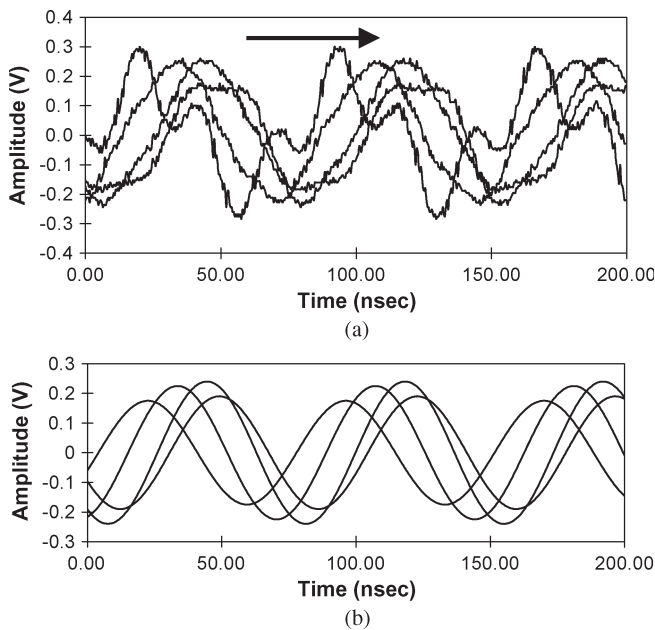Fig. 8. PR3 helicon plasma source. All dimensions are in centimeters.



Fig. 9. (a) Raw signals from the free column coil array showing travelling waves. (b) Fundamental component only. Distances from the antenna: 20, 28, 36, and 44 cm. The arrow indicates the direction of travel.

*3) Travelling-Wave Amplitudes:* For the PR3 source, the movable mesh baffle acts as a short-circuit termination so that the cavity formed between the baffle and the antenna should lead to large amplitude travelling waves when its length is an odd number of quarter wavelengths long. Similarly, the amplitudes should be small for a half-wavelength cavity. The signals from the coils were filtered to yield only their fundamental component, as shown, for example, in Fig. 9(b). The amplitude and wavelength of the fundamental were measured for RF power levels between 600 and 2100 W and cavity lengths from 15 to 40 cm. As the power level increased, the electron density increased almost linearly, and the wavelength decreased. The wavelength ranged from ~70 cm at 600 W to ~28 cm at 2100 W. The amplitudes of the waves ranged from 0.27 to 0.59 V p-p and generally increased with power level. However, for a given cavity length, as the wavelength decreased to a point where $\lambda/2 \sim l$, then there was a marked decrease in amplitude.
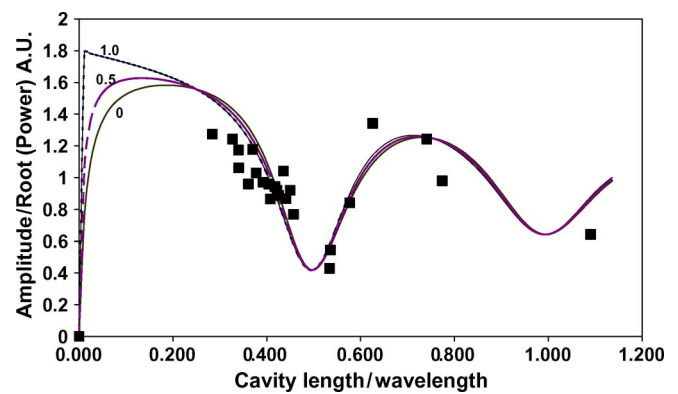


Fig. 10. Travelling-wave amplitudes normalized by the square root of the power density as a function of cavity length/wavelength: (Diamonds) Experiment and (solid line) theory.

Fig. 10 shows a composite plot that summarizes the findings. The amplitudes plotted on the vertical axis have been scaled by dividing them by the square root of the power density to allow for different applied power levels. The horizontal axis plots the ratio of cavity length to wavelength for a variety of combinations of cavity length and wavelength. Despite the wide range of power levels, wavelengths, and cavity lengths, the normalization for both the vertical and horizontal axes has collapsed the results onto a single curve.

The results show a clear dip in the amplitude when the cavity is half-a-wavelength long, leading to a node under the antenna, a low input impedance to the cavity, and so poor coupling of power into the travelling waves. Observations of the travelling-wave fields also show that the amplitude of these waves is large when there is an approximate antinode under the antenna which corresponds to cavity lengths equal to an odd number of 1/4 wavelengths.

The theoretical curves shown in Fig. 10 are based on (16) and assume that the amplitude is proportional to the square root of the power applied to the travelling waves. The ratio of the attenuation constant to axial wavenumber $\alpha/\beta$ has been adjusted to give the best fit between theory and experiment with a value of $0.1 \pm 0.03$. Based on (16), three curves have been plotted for values of the ratio of reactance to the resistance of the wave impedance $\eta_I/\eta_R = m(\alpha/\beta)$, where $m = 0$, 0.5, and 1.0. These curves show that, except at very short cavity
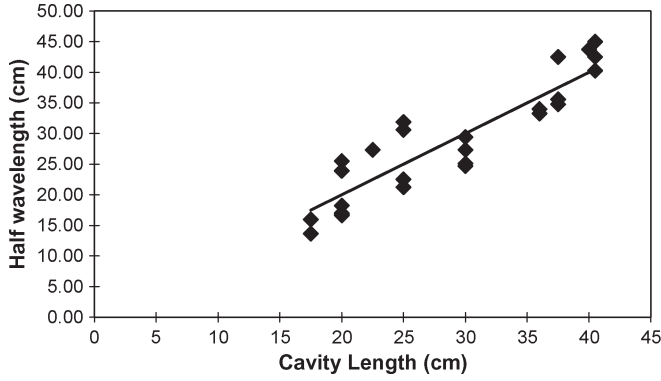
Fig. 11. Half wavelength just below the cavity mode transition from the $\lambda/4$ mode to the $3\lambda/4$ mode as a function of cavity length. The line $\lambda/2 = l$ for a node under the antenna is shown for comparison. Magnetic field: 400 G.



Fig. 12. Experimental ratio of attenuation $(\alpha)$ to axial wavenumber $(\beta)$ as a function of a scaling function for $\alpha/\beta$ [see (41)]. The numbers adjacent to the points refer to the reference from which the data were derived.

lengths, the reactance has little effect on the curves due to the damping effect of the ratio of $T_I/T_R$ as the cavity length increases.

*4) Stable and Unstable Operation:* Stable operation occurred when the cavity length was close to an odd number of quarter wavelengths, giving a node at the baffle and an approximate antinode at the antenna. The occurrence of a third harmonic component, as in Fig. 9, is consistent with this view as it also leads to a resonance in the cavity region.

For most cavity lengths, the cavity impedance is large compared with the travelling-wave impedance. However, if the length is $\sim 1/2\lambda$, the impedance is small. Thus, most of the power goes to the cavity, and the operation of the source becomes unstable. Large amplitude travelling waves therefore require the cavity to be $\sim 1/4\lambda$ or $3/4\lambda$ long.

Fig. 11 shows the half wavelength of the helicon waves, inferred from (36), just below the cavity transition from the $1/4\lambda$ to the $3/4\lambda$ mode compared with the line for which $\lambda/2 = l$ for a field of 400 G, pressures between 2 and 4 $\mu$bar, and power levels from 600 to 2100 W. The wavelengths cluster around this line and thus confirm that the transition occurs when an approximate node exists under the antenna. This result is consistent with the findings in Fig. 10 for the travelling waves. The scatter about this line may be attributed to the fact that the line represents a region of instability. The transition also depends on the tuning of the matching network. If tuned in anticipation of the conditions on the other side of the transition, then the transition is facilitated. These results further demonstrate the importance of choosing the correct length for the cavity if stable operation of the source is to be achieved.

*5) Attenuation:* For a helicon wave, the ratio of the attenuation coefficient to the axial wavenumber, in terms of the notation used in this paper, is given by [15]

$$\frac{\alpha}{\beta} = \frac{\nu_{\text{eff}}}{\omega_{ce}} \frac{\left[1 + (k_\perp/\beta)^2\right]^{3/2}}{\left[2 + (k_\perp/\beta)^2\right]} \qquad (37)$$

where $\nu_{\text{eff}}$ is the effective collision frequency, $\omega_{ce} = eB/m$ is the electron cyclotron frequency, $k_\perp = \chi/a$ is the radial

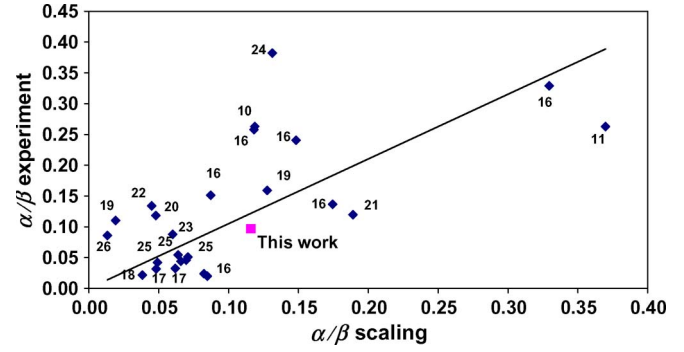wavenumber, $a$ is the radius of the plasma vessel, and $\chi \approx 3.1$ for the $n = 1$ radial mode.

Similarly, the simple helicon dispersion relation can be written as [15]

$$\beta^2 = \frac{k_0^2 \omega_p^2}{\omega \omega_{ce}} \left(1 + \left(\frac{k_\perp}{\beta}\right)^2\right)^{-1/2} \qquad (38)$$

where $\omega_p$ is the plasma frequency and $k_0$ is the free-space wave vector.

In most helicon discharges, $(k_\perp/\beta)^2 \gg 1$ so that (37) and (38) reduce to

$$\frac{\alpha}{\beta} \approx \frac{\nu_{\text{eff}} k_\perp}{\omega_{ce}} \frac{1}{\beta} \qquad (39)$$

$$\beta \approx \frac{k_0^2 \omega_p^2}{\omega \omega_{ce} k_\perp}. \qquad (40)$$

Substitution of (40) into (39) and converting to more physical parameters give

$$\frac{\alpha}{\beta} = \frac{m}{\mu_0 e^2} \left(\frac{\chi}{a}\right)^2 \frac{\nu_{\text{eff}}}{\omega n_0}. \qquad (41)$$

To test this scaling function for $\alpha/\beta$, a number of papers that include data on the decay of helicon waves have been consulted to determine experimental values for $\alpha/\beta$, in terms of the parameters $\chi/a$, $\omega$, and $n_0$ [10], [11], [16]–[26]. In some cases, explicit values of the parameters are not reported but have been inferred from the relevant graphs. The papers investigate a wide variety of processes to explain the absorption mechanisms in different regimes, including electron trapping in the axial electric field of traveling waves [10], electron–neutral and electron–ion collisions [16], [17], collisionless Landau damping [9, p. 442], resonance absorption through wave trapping by density gradients [11], and parametric instabilities leading to ion-sound and Trivelpiece-Gould waves [21]–[23]. Rather than attempting to deal with each of these mechanisms in detail, for the purposes of (41), a single effective collision frequency $\nu_{\text{eff}} = 3 \times 10^8 \text{ s}^{-1}$ has been selected to give the best overall match. Fig. 12 shows the experimental values of $\alpha/\beta$ as a function of the $\alpha/\beta$ scaling given by the right-hand side of (41).

The numbers adjacent to the points show the reference from which the data were derived. In making this comparison, we recognize that the results can be specific to a particular experiment and that factors such as the details of the geometry, the uniformity, or otherwise, of the magnetic field, whether the helicon source is connected to a larger diffusion chamber, the operating pressure, the type of antenna, and the shape of the radial density profile may all affect the comparisons between experiments. Despite these differences and the considerable scatter, the results show a general trend with high-density discharges generally having lower values for $\alpha/\beta$ than low-density discharges.

We have also plotted our value of $\alpha/\beta = 0.1$ using the same scaling function, which shows that it is generally consistent with other investigations.

## V. Conclusion

In many applications of plasma to industrial situations, a wave-heated plasma source of finite length is often coupled to a much larger processing chamber or plasma column. In such applications, it is important to maximize the power transferred to the processing chamber by the travelling waves generated by the source. In this paper, we have shown that an analysis where the plasma is modeled as a lossy finite length transmission line coupled at the launcher (antenna) to an infinite lossy transmission line produces a good agreement with the experiment. For a cavity terminated in a conducting end plate to the plasma vessel, which corresponds to a transmission line with a short-circuit load, we find that the power delivered to the travelling waves is a maximum when the distance from the end plate to the launcher is an odd number of 1/4 wavelengths. Based on standard transmission line theory, this means that the input impedance to the transmission line is very large compared with the input impedance to the infinite line. Thus, most of the power applied to the launcher should be directed to the travelling waves. For the same situation if the transmission line is 1/2 wavelength long, then, for a short-circuit load, its input impedance should be very low with most of the power directed toward the finite line.

We have also found that if the end of the vessel is an insulator corresponding to an open-circuit load and if the length of the line is 1/2 wavelength long, then its input impedance is again very high, meaning that most of the power is directed to the travelling waves.

We have also demonstrated that simple expressions for the attenuation coefficient for both surface- and helicon-wave discharges yield values that are consistent with those required to fit the theory to the experimental data. In addition, the dispersion relations for these two types of waves lead to wavelengths that are in accord with the experimental observations.

The outcomes of this investigation mean that, when designing a plasma source for geometries similar to those described in this paper, the first step is to use the appropriate dispersion relation to calculate the wavelength based on the anticipated electron number density. The power delivered by the travelling waves to the processing region can be maximized by a suitable choice of the distance between the launcher and the end of the

source, bearing in mind the conducting or insulating nature of the end cap and the anticipated wavelength.

## References

[1] K. K. Chi, T. E. Sheridan, and R. W. Boswell, "Resonant cavity modes of a bounded helicon discharge," *Plasma Sources Sci. Technol.*, vol. 8, no. 3, pp. 421–431, Aug. 1999.

[2] M. Nisoa, Y. Sakawa, and T. Shoji, "Plasma production by $m = 0$ standing helicon waves," *Jpn. J. Appl. Phys.*, vol. 39, no. 5A, pp. L429–L432, May 2000.

[3] J. P. Rayner and A. D. Cheetham, "Helicon modes in a cylindrical plasma source," *Plasma Sources Sci. Technol.*, vol. 8, no. 1, pp. 79–87, Feb. 1999.

[4] S. Nonaka, "Mode coupling phenomena of longitudinal quarter-wavelength resonance of a plasma column produced by surface waves," *J. Phys. Soc. Jpn.*, vol. 59, no. 5, pp. 1623–1632, May 1990.

[5] M. Moison and Z. Zakrzewski, "Plasma sources based on the propagation of electromagnetic surface waves," *J Phys. D, Appl. Phys.*, vol. 24, no. 7, pp. 1025–1048, Jul. 1991.

[6] G. G. Borg, J. H. Harris, M. N. Martin, D. Thorncraft, R. Miliken, D. G. Miljak, B. Kwan, T. Ng, and J. Kircher, "Plasma as antennas: Theory, experiment and applications," *Phys. Plasmas*, vol. 7, no. 5, pp. 2198–2202, Jul. 2000.

[7] J. P. Rayner, A. P. Whichello, and A. D. Cheetham, "Physical characteristics of plasma antennas," *IEEE Trans. Plasma Sci.*, vol. 32, no. 1, pp. 269–281, Feb. 2004.

[8] A. J. Perry, D. Vender, and R. W. Boswell, "The application of the helicon source to plasma processing," *J. Vac. Sci. Technol. B, Microelectron. Process. Phenom.*, vol. 9, no. 2, pp. 310–316, Mar. 1991.

[9] M. A. Lieberman and A. J. Lichtenberg, *Principles of Plasma Discharges and Materials Processing.*, 1st ed. New York: Wiley, 1994.

[10] A. R. Ellingboe and R. W. Boswell, "Electron beam pulses produced by helicon-wave excitation," *Phys. Plasmas*, vol. 2, no. 6, pp. 1807–1809, Jun. 1995.

[11] M. I. Panevsky and R. D. Bengtson, "Characterization of the resonant electromagnetic mode in helicon discharges," *Phys. Plasmas*, vol. 11, no. 9, pp. 4196–4205, Sep. 2004.

[12] D. K. Cheng, *Field and Wave Electromagnetics.*, 2nd ed. Reading, MA: Addison-Wesley, 1989.

[13] J. P. Rayner, A. D. Cheetham, and G. N. French, "Radio frequency matching for helicon plasma sources," *J. Vac. Sci. Technol. A, Vac. Surf. Films*, vol. 14, no. 4, pp. 1–8, Jul./Aug. 1996.

[14] A. D. Cheetham and J. P. Rayner, "Characterization and modeling of a helicon plasma source," *J. Vac. Sci. Technol. A, Vac. Surf. Films*, vol. 16, no. 5, pp. 2777–2784, Sep./Oct. 1998.

[15] F. F. Chen, "Plasma ionization by helicon waves," *Plasma Phys. Control. Fusion*, vol. 33, no. 4, pp. 339–364, Apr. 1991.

[16] D. A. Schneider, G. G. Borg, and I. V. Kamenski, "Measurements and code comparison of wave dispersion and antenna radiation resistance for helicon waves in a high density cylindrical plasma source," *Phys. Plasmas*, vol. 6, no. 3, pp. 703–712, Mar. 1999.

[17] M. Light, I. D. Sudit, F. F. Chen, and D. Arnush, "Axial propagation of helicon waves," *Phys. Plasmas*, vol. 2, no. 11, pp. 4094–4102, Nov. 1995.

[18] D. G. Miljak and F. F. Chen, "Helicon wave excitation with rotating antenna fields," *Plasma Sources Sci. Technol.*, vol. 7, no. 1, pp. 61–74, Feb. 1998.

[19] S. M. Tysk, C. M. Denning, J. E. Scharer, and K. Akhtar, "Optical, wave measurements, and modelling of helicon plasmas for a wide range of magnetic fields," *Phys. Plasmas*, vol. 11, no. 2, pp. 876–887, Mar. 2004.

[20] X. M. Guo, J. Scharer, Y. Mouzouris, and L. Louis, "Helicon experiments and simulations in nonuniform magnetic field configurations," *Phys. Plasmas*, vol. 6, no. 8, pp. 3400–3407, Aug. 1999.

[21] K. Niemi and M. Krämer, "Helicon mode formation and radio frequency power deposition in a helicon-produced plasma," *Phys. Plasmas*, vol. 15, no. 7, pp. 073 503-1–073 503-11, Jul. 2008.

[22] B. Lorenz, M. Krämer, V. L. Selenin, and Y. M. Aliev, "Excitation of short-scale fluctuations by parametric decay of helicon waves into ion-sound and Trivelpiece-Gould waves," *Plasma Sources Sci. Technol.*, vol. 14, no. 3, pp. 623–635, Aug. 2005.

[23] M. Krämer, Y. M. Aliev, A. B. Altukhov, A. D. Gurchenko, E. Z. Gusakov, and K. Niemi, "Anomalous helicon wave absorption and parametric excitation of electrostatic fluctuations in a helicon-produced plasma," *Plasma Phys. Control. Fusion*, vol. 49, no. 5A, pp. A167–A175, May 2007.

[24] J. Scharer, A. Degeling, G. Borg, and R. Boswell, "Measurements of helicon wave propagation and Ar II emission," *Phys. Plasmas*, vol. 9, no. 9, pp. 3734–3742, Sep. 2002.

[25] R. T. S. Chen, R. A. Breun, S. Gross, N. Hershkowitz, M.-K. J. Hsieh, and J. Jacobs, "Experimental studies of multimode helicon plasma waves," *Plasma Sources Sci. Technol.*, vol. 4, no. 3, pp. 337–344, Aug. 1995.

[26] T. Enk and M. Krämer, "Radio frequency power deposition in a high-density helicon discharge with helical antenna coupling," *Phys. Plasmas*, vol. 7, no. 10, pp. 4308–4319, Oct. 2000.

**John Phillip Rayner** received the Ph.D. degree in physics in the field of hypervelocity aerodynamics from the Australian National University (ANU), Canberra, Australia, in 1974.

Since then, he has combined his research work with a career in higher education in physics and engineering principally at the University of Canberra, Canberra, where he was the Head of the Faculty of Information Sciences and Engineering. He is currently an Adjunct Professor with the same faculty and also a Visiting Fellow with the ANU's Centre for the Public Awareness of Science. His research interests include plasma engineering, science education, and the history of exploration geophysics in Australia.

Dr. Rayner received the award of Member of the Order of Australia in 2007 for services to physics and science education.

**Andrew Desmond Cheetham** (M'99) received the Ph.D. degree in plasma physics from Flinders University, Adelaide, South Australia.

After receiving the degree, he spent 15 years working in the field of plasma measurement systems in the national fusion energy research laboratories of the University of Stuttgart, Stuttgart, Germany, École Polytechnique Fédérale de Lausanne, Lausanne, Switzerland, and Australian National University, Canberra, Australia, and ultimately as a Principal Scientific Officer with the Joint European Torus (JET) Joint Undertaking, Culham, U.K. In 1990, he returned to Australia and then joined the School of Electronics Engineering and Applied Physics, University of Canberra, Canberra, where he has taught physics, electronics, power systems, signal processing, computer-controlled instrumentation, and automatic control systems. Since 2007, he has been the Pro Vice-Chancellor (Research) with the University of Western Sydney, Sydney, Australia.